Review Paper

Experiments in Fluids 29 (2000) 103–116 © Springer-Verlag 2000

Stereoscopic particle image velocimetry

A. K. Prasad

Abstract Stereoscopic particle image velocimetry (PIV) employs two cameras to record simultaneous but distinct off-axis views of the same region of interest (illuminated plane within a flow seeded with tracer particles). Sufficient information is contained in the two views to extract the out-of-plane motion of particles, and also to eliminate perspective error which can contaminate the in-plane measurement. This review discusses the principle of stereoscopic PIV, the different stereoscopic configurations that have been used, the relative error in the out-of-plane to the in-plane measurement, and the relative merits of calibration-based methods for reconstructing the three-dimensional displacement vector in comparison to geometric reconstruction. It appears that the current trend amongst practitioners of stereoscopic PIV is to use digital cameras to record the two views in the angular displacement configuration while incorporating the Scheimpflug condition. The use of calibration methods has also gained prominence over geometric reconstruction.

1 Introduction

The method of using two cameras to obtain depth-perception has been practiced for several decades in various engineering applications. In fact, such twin camera systems mimic the binocular vision that enables human beings to distinguish between objects near and far. Essentially, a single view cannot resolve the out-of-plane dimension of the object field. Instead, the out-of-plane component is actually projected on to the object plane and causes a perspective error in the in-plane component. When measuring three-dimensional particle displacements, one may characterize this situation as having three unknowns $(\Delta x, \Delta y, \Delta z)$ with the single view providing only two equations. The addition of a second, different view, provides two additional equations which may be used to solve for the three-dimensional information. Our eyes record two such off-axis views simultaneously and the brain is able to combine the two views together in real time to provide three-dimensional vision.

This review paper only considers the measurement of three-dimensional vectors on planar domains. According to the classification proposed by Hinsch (1995) a measurement system can be labeled as (k, l, m) where $k = 1, 2, 3$ indicates the number of velocity components measured, $l = 0, 1, 2, 3$ indicates the number of spatial dimensions of the measurement domain, and $m = 0, 1$ indicates instantaneous or continuous time recording, respectively. The focus of this review is exclusively on the (3, 2, 0) method. In particular, we will examine in detail stereoscopic techniques that employ high-density correlation PIV. Alternative (3, 2, 0) methods that employ other (non-stereoscopic) strategies will also be mentioned; new users are confronted with a variety of choices and it is useful to compare and contrast stereoscopic PIV with such other methods.

All stereoscopic systems, despite the wide variety in configurations, must satisfy the basic requirement of recording two simultaneous, but different views of the same object. The two views are then combined using one of an assortment of algorithms to reconstruct the three-dimensional field. This review paper is organized as follows. First, we will examine the need for stereoscopic systems by analyzing the shortcomings of conventional single camera PIV, and describe how these shortcomings may be overcome by the addition of a second camera. Next, we will review several stereoscopic configurations that have been used along with their relative merits. In this section, we will also mention alternative (non-stereoscopic) methods of obtaining three-dimensional vectors on planar domains. Next, the error analysis of stereoscopic systems will be discussed. Finally, the important topic of reconstruction of the three dimensional field will be presented.

Figure 1 shows the conventional single camera PIV arrangement wherein the camera axis is perpendicular to the illuminated plane in order to obtain the in-plane velocity components. A particle with initial position $\mathbf{x}_i = (x, y, 0)$ forms an image at $\mathbf{X}_i = (-M_n x, -M_n y, 0)$ where the nominal magnification, $M_n = d_i/d_o$. Here, d_o is the object distance to the middle of the light sheet, and d_i is the corresponding image distance. It should be noted that Fig. 1 depicts the motion of only one particle, and secondly, that this particle is initially located exactly on the object plane ($z = 0$, the mid-plane of the light sheet). In reality, each PIV measurement averages the motion of all particles lying in an interrogation volume produced by the intersection of the light sheet with the back-projection of the interrogation spot onto the object plane. Second, these particles cannot obviously be constrained to start their motions from the object plane ($z = 0$) in a real flow.

Received: 15 April 1999/Accepted: 1 February 2000

A. K. Prasad
Department of Mechanical Engineering
University of Delaware, Newark, DE 19716-3140, USA

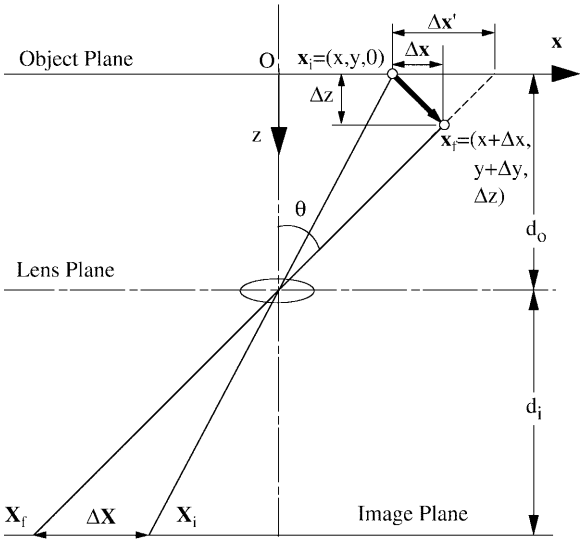

Fig. 1. Error in the measurement of in-plane displacements due out-of-plane motion using a single camera

However, as shown by Prasad and Adrian (1993a), the process of integrating the contributions of multiple particles embedded uniformly throughout the interrogation volume reduces the physical problem to the situation depicted in Fig. 1 with an error of order $(\Delta z_o/d_o)^2$ where Δz_o is the thickness of the light sheet. For a typical PIV recording, $\Delta z_o \approx 1$ mm and d_o is hundreds of millimeters, so this error is negligible. Therefore, subsequent figures and analysis in this paper will only consider the motion of a single particle whose initial location is at $z = 0$.

Referring again to Fig. 1, when the particle under consideration moves to a final position of $\mathbf{x}_f = (x + \Delta x, y + \Delta y, \Delta z)$ it forms an image at $\mathbf{X}_f = (-M_f(x + \Delta x), -M_f(y + \Delta y), 0)$ where $M_f = d_i/(d_o - \Delta z)$. The resulting image displacement vector, as recorded on the image plane, is:

$$\begin{aligned}\mathbf{\Delta X} &= \mathbf{X}_f - \mathbf{X}_i \\ &= \left(-M_n \frac{\Delta x + x\Delta z/d_o}{1 - \Delta z/d_o}, -M_n \frac{\Delta y + y\Delta z/d_o}{1 - \Delta z/d_o}, 0\right)\end{aligned} \tag{1}$$

Figure 1 shows that particles which are not located directly on the camera axis and which experience out-of-plane motion, Δz, will record displacements, $\mathbf{\Delta X}$, which do not match the true in-plane displacements, $(\Delta x, \Delta y)$. Rather, $\mathbf{\Delta X}$ maps back to an *apparent in-plane* displacement of $\mathbf{\Delta x}' = -\mathbf{\Delta X}/M_n$ on the object plane, i.e.,

$$\mathbf{\Delta x}' = \frac{\mathbf{\Delta X}}{-M_n} = \left(\frac{\Delta x + x\Delta z/d_o}{1 - \Delta z/d_o}, \frac{\Delta y + y\Delta z/d_o}{1 - \Delta z/d_o}, 0\right)$$

The relative error between the true and the apparent in-plane displacement, ϵ, is called the perspective error.

$$\begin{aligned}\epsilon = (\epsilon_x, \epsilon_y) &= \left(\frac{\Delta x'}{\Delta x} - 1, \frac{\Delta y'}{\Delta y} - 1\right) \\ &= \left(\frac{\Delta z}{\Delta x}\tan\,\theta_x, \frac{\Delta z}{\Delta y}\tan\,\theta_y\right)\end{aligned} \tag{2}$$

where θ_x and θ_y are projections of θ on the x-z and y-z planes respectively. Perspective error can significantly contaminate in-plane measurements when the relative out-of-plane component is large, as well as when the angle subtended by the particle to the camera-axis, θ, is large. For example, an off-axis angle of 5° subtended by the edge of the region of interest to the lens (θ in Fig. 1) in single camera PIV can cause an error of about 10% in the in-plane measurement when the in-plane and out-of-plane displacements are of similar magnitude. Relatively larger out-of-plane displacements will produce proportionally greater perspective errors. This result was also provided by Jacquot and Rastogi (1981) for the displacement of solid surfaces.

Stereoscopic PIV eliminates this problem by acquiring two simultaneous views along different off-axis directions as shown in Fig. 2. The apparent displacements recorded by each camera, $\mathbf{\Delta X_1}$ and $\mathbf{\Delta X_2}$, are later combined to obtain the correct in-plane displacement, $(\Delta x, \Delta y)$, and more importantly, the out-of-plane displacement, Δz.

2
Stereoscopic configurations

Commonly used stereoscopic systems may be broadly classified according to (i) translation systems, also known as lateral displacement, and (ii) rotational systems, also known as angular displacement (Fig. 3). These major systems will be addressed first along with their variations. Additional stereoscopic configurations which cannot be strictly classified as translational or rotational systems will be discussed next. Finally, we will mention alternative (non-stereoscopic) methods of obtaining three-dimensional vectors on planar domains at the end of this section.

2.1
Translation systems

In the translation system, the axes of both cameras are placed parallel to each other, such that they are both orthogonal to the light sheet. This system is depicted in Fig. 2 and in Fig. 3a. Although Fig. 2 shows the two cameras to be symmetric with respect to the system axis, such symmetry is not necessary – for example, the separation of each lens from the system axis and/or the magnification of each camera could be different. However, symmetric systems are more conveniently implemented. The translation configuration was described by Jacquot and Rastogi (1981), Sinha (1988), Gauthier and Riethmuller (1988), and Lawson and Wu (1997a), and was used for measurements by Arroyo and Greated (1991), Sinha and Kuhlman (1992), Prasad and Adrian (1993a, b), Synnergren (1997), Soloff et al. (1997), Liu et al. (1997), and Lecerf et al. (1999).

The primary advantage of the translation method is its simplicity. Because the object plane, lens plane, and image plane are all parallel to each other, the image field enjoys uniform magnification. Furthermore, in the absence of refractive-index jumps along the optical path from the lens to the object plane (such as that caused by recording through a thick liquid layer, for example), the particle image quality is not compromised. Good image focus is achieved without the need to reduce the aperture beyond

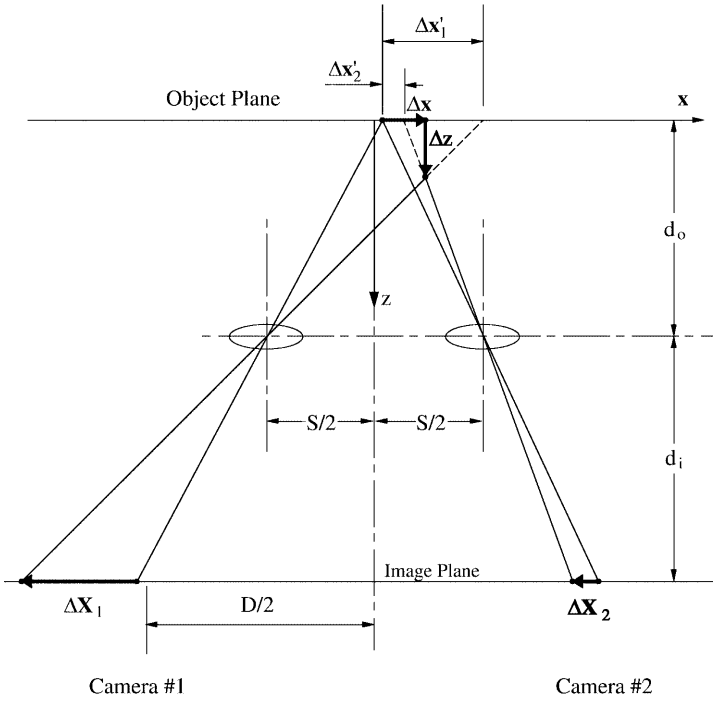

Fig. 2. Schematic of stereocamera in the translation configuration

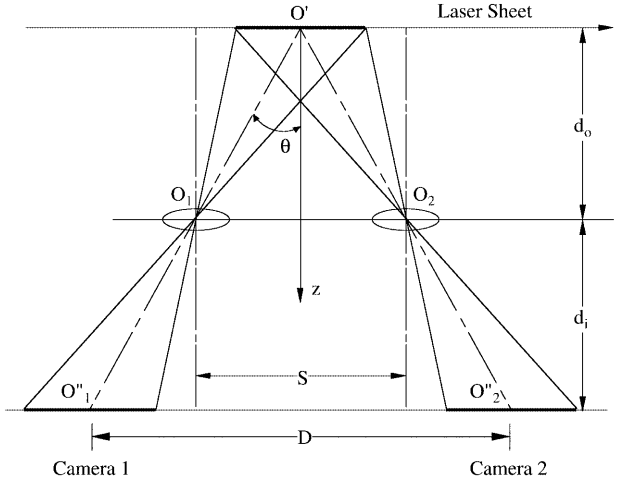

(a) Translation system

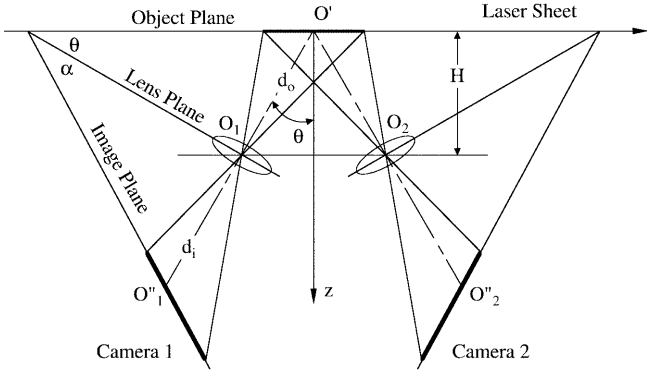

(b) Angular displacement system

Fig. 3a, b. Two basic configurations for stereoscopic PIV systems: **a** translation method, **b** angular-displacement method

what is used in single camera PIV (i.e., the depth-of-field requirement is unchanged). The two views can be readily superposed without additional manipulations that a non-uniform magnification would necessitate. In addition, the spatial resolution of the combined field will be identical to that of the two individual views.

One of the objections raised by Gauthier and Riethmuller (1988) to the translation method is the small "common area" viewed by each camera. However, the common area can be maximized by off-setting each sensor frame away from the lens-axis (see Fig. 3a) such that:

$$D = (1 + M_n)S$$

where D is the distance between the centers of the sensors, and S is the distance between the camera-lens axes. It should be noted, however, that such an off-set may be difficult to enforce with CCD cameras due to vignetting caused by the camera body.

A more serious difficulty with the translation system is that there is an upper bound to the off-axis angle θ subtended by the center of the region of interest to the center of the lens (see Fig. 3a). This restriction arises purely from the design of the lens; if the lenses are separated by a value that is too large for a given d_o, the lens performance degrades as it is forced to operate at the outer limit of its specification. It will be shown later that the relative error in the out-of-plane component decreases when the off-axis angle increases, implying that the translation system is somewhat limited in the accuracy of the out-of-plane component. Results obtained by Prasad and Adrian (1993a), Arroyo and Greated (1991), and Soloff et al. (1997) indicate that the out-of-plane error exceeds the in-plane error by a factor of 3 to 4 for typical translation systems, corresponding to a half-angle $\theta \approx 15^\circ$. In the case of Prasad and Adrian (1993a), the in-plane and out-of-

plane rms errors amounted to 1 μm and 4 μm respectively, at an object distance of 247 mm.

The geometric relationship between the true particle displacements (Δx, Δy, and Δz), and the apparent displacements measured by camera no. 1 ($\Delta X_1, \Delta Y_1$), and camera no. 2 ($\Delta X_2, \Delta Y_2$) can be easily derived by examining Fig. 2 and are presented below.

$$\Delta z = \frac{-d_o(\Delta X_1 - \Delta X_2)}{M_n S - (\Delta X_1 - \Delta X_2)} \tag{3}$$

$$\Delta x = \frac{\Delta X_1(x - S/2) - \Delta X_2(x + S/2)}{M_n S - (\Delta X_1 - \Delta X_2)} \tag{4}$$

$$\Delta y = \frac{-y\Delta z}{d_o} + \frac{\Delta Y_1 + \Delta Y_2}{2M_n}\left[\frac{\Delta z}{d_o} - 1\right] \tag{5}$$

As mentioned in Sect. 1, the two views provide four equations for three unknowns. The additional equation may be used to improve the accuracy of Δy as has been done above by averaging the Δy determined by each camera. Similar equations for translation systems have been provided by other workers mentioned earlier.

A variation on the conventional translation arrangement used by Arroyo and Greated (1991) involved the placement of one pair of mirrors M_1 between the object plane and the lens plane, and a second pair between the lens plane and the image plane M_2. These mirrors fold the light scattered along off-axis angles such that the two views are recorded adjacent to each other on the *same* sensor. The center of the region of interest O′ maps to two adjacent regions O_1'' and O_2'' as shown in Fig. 4. This system requires only one lens and one sensor.

Prasad and Adrian (1993a, b) applied the translation configuration to liquid flows, wherein the object plane resided within a thick liquid layer. The refractive index jump at the liquid-air interface caused some difficulties: (i) aberrations due to the interface caused particle images to be radially distorted, and (ii) the plane over which particles could be obtained in acceptable focus was no longer parallel to the object plane but had to be tilted at some angle to it. The first problem forced the use of small

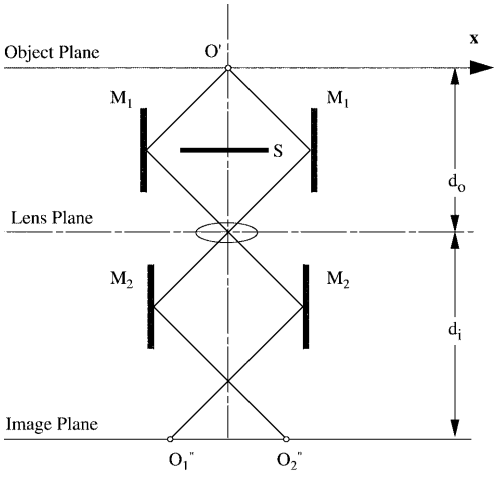

Fig. 4. Translation configuration using a single camera (adapted from Arroyo and Greated 1991)

f-numbers, and the second caused some non-uniformity in the magnification. Therefore, the basic advantages of using the translation system were somewhat diminished in this application. Prasad and Adrian (1993a) implemented modifications in hardware and software to successfully accomplish the three-dimensional measurements below a disk rotating in a tank of glycerine. Using the same arrangement, Prasad and Adrian (1993b) obtained three-dimensional measurements in turbulent thermal convection at a Rayleigh number of about 2×10^7.

2.2 Rotational systems

The restriction on θ imposed by the translation arrangement is removed in rotational systems. As shown in Fig. 3b the two camera axes are no longer parallel to each other but are rotated such that the two axes intersect the object plane at the system axis. Now the angle θ may be increased to much larger values without incurring problems associated with lens performance, thereby allowing greater accuracy in the out-of-plane component. However, the magnification is no longer uniform over the field of view. Furthermore, as shown in Fig. 3b, the image plane has to be further rotated with respect to the lens plane by an angle α such that the object plane, lens plane and image plane are colinear. This requirement, known as the Scheimpflug condition (Altenhofen 1952) ensures that all particles in the object field will be in good focus in the image plane. However, the Scheimpflug condition exacerbates the non-uniformity in magnification. Figure 5 illustrates the variation in magnification across the object plane for a Scheimpflug system, for off-axis half-angles of (a) 15°, (b) 30°, and (c) 45°, and nominal magnifications M_n between 0.2 and 1.0 in steps of 0.2. (For the Scheimpflug system $M_n = \tan\alpha / \tan\theta$.) The distance along the horizontal axis in the object plane, x, is normalized by the nominal object distance d_o (see Fig. 3b) and the resulting local magnification is normalized by the nominal magnification (realized at $x/d_o = 0$). It is apparent that the non-uniformity increases with $|x|$, θ, and M_n. The data in Fig. 5 pertains only to the x-axis; for a given x, the non-uniformity increases with distance from the x-axis.

In addition to non-uniformity, the angular displacement arrangement depicted in Fig. 3b produces image fields which are oppositely stretched. This effect is shown in Fig. 6, where square interrogation spots in the image plane map to oppositely stretched, and differently located, trapezoids in the object plane. Obviously, a reverse mapping would cause a cartesian grid in the object plane to be oppositely stretched in each image plane as well. As indicated by the shaded regions, it is impossible to directly combine information from each view in the image plane without first interpolating the data on to a common grid. It should be noted that the two distorted grids in Fig. 6 are maximally overlapped, in that, their vertical edges coincide. In order to achieve such a maximum overlap, the two cameras will need to be moved somewhat closer together than Fig. 3a indicates, such that their axes intersect not at the object plane but in front of it (Westerweel and van Oord 1999).

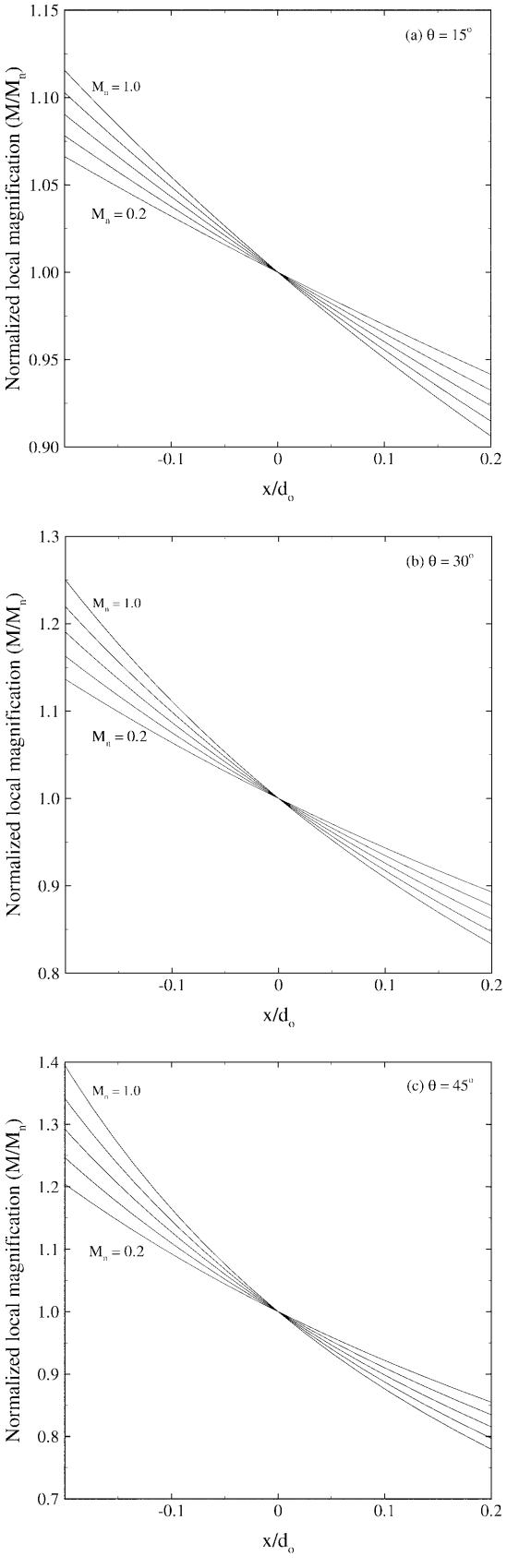

Fig. 5a–c. Non-uniformity in magnification across the object plane in the Scheimpflug system for nominal magnifications varying between 0.2 and 1.0 in steps of 0.2: **a** $\theta = 15°$, **b** $\theta = 30°$, **c** $\theta = 45°$

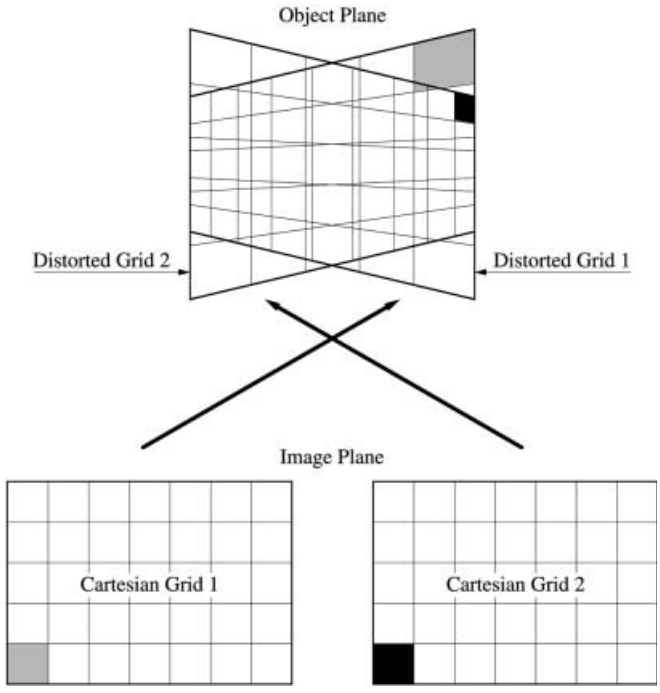

Fig. 6. Opposite stretching of a cartesian grid in the image plane when mapped onto the object plane

It is possible to employ the angular displacement configuration without enforcing the Scheimpflug condition (by setting $\alpha = 0$) which reduces somewhat the non-uniformity in magnification. In this case, particles can be obtained in good focus only by ensuring that the depth-of-field δz of the system is large enough to account for the varying object distance. Adrian (1991) gives:

$$\delta z = 4(1 + M_{\mathrm{n}}^{-1})^2 f^{\#2} \lambda$$

where M_{n} is the camera magnification, and λ is the wavelength of the illuminating laser. For a given magnification, a large depth-of-field can only be obtained at the cost of increasing the f-number, $f^{\#}$, implying that a smaller fraction of the light scattered by the particles will reach the sensor. Such a system was described by Gauthier and Riethmuller (1988) and employed by Westerweel and Nieuwstadt (1991), Grant et al. (1991), and Lawson and Wu (1997b). The Scheimpflug condition was suggested by Hinsch (1995), and Prasad and Jensen (1995), and subsequently employed by Zang and Prasad (1997), Willert (1997), Bjorkquist (1998), Westerweel and van Oord (1999), and Hill et al. (1999).

Willert (1997) used a variation of the Scheimpflug angular displacement system in which the two cameras were placed on *either* side of the light sheet (Fig. 7). Two benefits accrue from this arrangement. First, by properly orienting the direction of propagation of the illuminating laser beam, it is possible to operate both cameras in forward scatter. Because scattering efficiency is significantly higher in forward scatter, both views can exploit higher (and equal) signal-to-noise ratios. Second, Willert's (1997) arrangement implies that both views will be stretched identically, rather than the opposite stretching for cameras

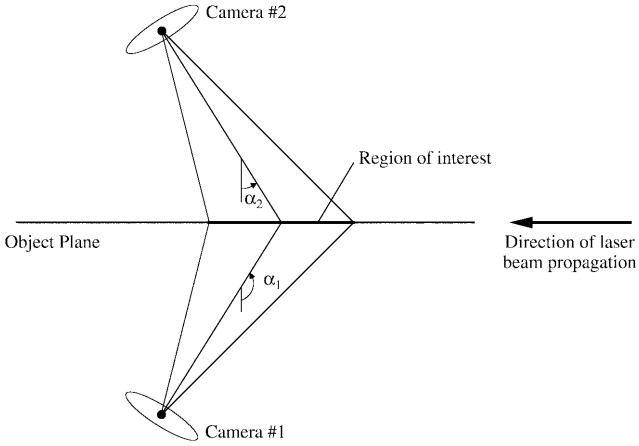

Fig. 7. Stereoscopic arrangement with cameras on either side of the light sheet (adapted from Willert 1997)

situated on the same side of the light sheet. However, the task of interpolating both views on to a cartesian grid still remains.

It is easily shown that the equations for the angular displacement system can be reduced to a form that is similar to the equations for the translation system. Such equations are given by Westerweel and Nieuwstadt (1991) and Lawson and Wu (1997a) for the non-Scheimpflug angular displacement stereocamera, and by Zang and Prasad (1997) for the Scheimpflug system. In fact, the equations presented by Westerweel and van Oord (1999) are identical to the translation equations. Willert (1997) also presents similar equations for cameras placed on either side of the light sheet.

On account of the large off-axis angles employed in angular displacement systems, debilitating aberrations can arise when recording is performed through a thick liquid layer. In fact, such aberrations are sometimes visible at the edges of the recorded domain even in single-camera PIV – wherein the camera axis is orthogonal to the light sheet – applied to a liquid flow (the edges may subtend an off-axis angle as small as a few degrees). These aberrations severely distort the particle images radially. Prasad and Jensen (1995) used ray-tracing to produce a graphical representation of such radial distortions. They then proposed the use of corrective optics in the form of a liquid prism to alleviate this problem. As shown in Fig. 8, a liquid prism (a thin-walled glass container which is filled with the test liquid), is constructed and attached to the wall of the test-section such that both cameras continue to enjoy an orthogonal orientation with respect to the liquid–air interface. The prism is located symmetrically with respect to the stereocamera, and orthogonal viewing is achieved when the half-angle of the stereoscopic system θ equals the angle subtended by the inclined walls of the liquid prism to the original interface. The nominal object distance for the system in Fig. 8 is given by

$$d_o = \frac{1}{\mu}(d_l + d_p)\cos\theta + d_a$$

The distances d_l, d_p, and d_a are all indicated in Fig. 8. μ is the refractive index of the test-liquid.

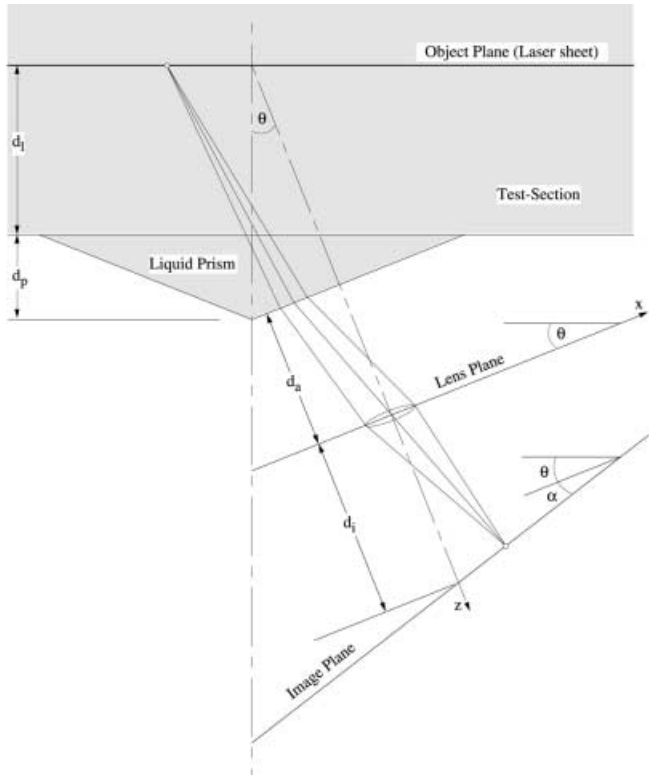

Fig. 8. Scheimpflug stereocamera with liquid prism (only one of two cameras in shown; adapted from Prasad and Jensen 1995)

In the absence of a liquid–air interface, sharp images are obtained when the object, lens, and image planes are colinear, as indicated in Fig. 3b. In the presence of a liquid–air interface, colinearity may not yield optimal images due to radial distortion. A small adjustment in the angle α and/or the nominal image distance will produce optimal images. Prasad and Jensen's (1995) ray-tracing analysis showed that the liquid prism is extremely efficient at reducing radial distortions arising from a liquid–air interface.

A second major advantage is that the liquid prism ensures paraxial recording; in the absence of paraxial recording, some amount of ray-tracing must be applied to modify the equations used to reconstruct the three-dimensional field. For example, Prasad and Adrian (1993a) have derived such modified equations for a situation in which paraxial recording was not employed.

Finally, when the stereoscopic half-angle θ is large enough to approach a value at which total internal reflection is imminent (49° for a ray emerging from water into air), then a liquid prism constitutes a simple remedy (Westerweel and van Oord 1999).

The liquid prism was employed by Westerweel and van Oord (1999) in a Scheimpflug system with half-angle $\theta = 45°$ to a turbulent boundary layer.

2.3
Other stereoscopic configurations

Gaydon et al. (1997) proposed a "hybrid" stereocamera which combines features of translational and rotational systems. Essentially, the hybrid system uses a small

translation between the camera axes, as well as a small inward rotation of the axes. The idea is to increase the off-axis angle beyond what is possible in an equivalent purely translation system, without increasing the non-uniformity in magnification to the level experienced by an equivalent purely rotational system. Gaydon et al. (1997) performed an optimization procedure to determine the ideal geometry for their application and concluded that the combination of a large angular displacement and relatively small translation gave the best result. They applied their stereocamera to an air-jet oriented perpendicular to the light sheet.

Grant et al. (1995) describe an in-line stereoscopic system, in which the two camera axes actually coincide, and are perpendicular to the object plane (similar to single camera two-dimensional PIV). As indicated in Fig. 9, the requirement for differing views is satisfied by using differing magnifications and object-distances for each camera. The in-line arrangement was facilitated with the use of a semi-silvered mirror placed along the common optical axis. One advantage of this system is that each particle forms images at the same angular location on each film, which speeded up particle matching for their particle tracking algorithm. However, the out-of-plane errors for this arrangement are quite large, especially as one approaches the center of the view field; in fact, in some neighborhood of the center, the technique cannot produce useful results. For regions removed from the center of the field of view, each camera views the same particle with different off-axis angles, however, the difference in angles is very small. Consequently, Grant et al. (1995) report out-of-plane errors $\sigma_{\Delta z}/d_o$ that are about 300 times larger than those reported by Prasad and Adrian (1993a).

2.4
Non-stereoscopic configurations

Three-dimensional vectors can be obtained on planar domains without resorting to stereoscopy. It is appropriate to review some of these alternative methods and compare them to stereoscopic PIV. We will limit the non-stereoscopic discussion to this section only which provides a brief introduction. The reader is referred to the original works for additional details.

Raffel et al. (1996) obtained three-dimensional vectors with a single camera by correlating particle images between three spatially staggered, but overlapping, parallel light sheets. This dual-plane correlation technique exploits the *height* of the correlation peak, which depends on the number of paired particle images, which inversely depends on the out-of-plane velocity component. Greater the out-of-plane velocity, greater the out-of-plane loss of pairs, and lower the correlation signal. Because the technique requires an out-of-plane loss of pairs to extract the out-of-plane component, spatial resolution is somewhat compromised as more particles must be included in each interrogation spot to increase the signal to noise ratio. Simulations of dual-plane PIV conducted by Raffel et al. (1996) revealed an error in the out-of-plane component between 4 and 8% of Δz_o, the light sheet thickness ($\Delta z_o = 2$ mm in their case). The technique offers the advantage of easy implementation, especially if the illuminating laser sheet possesses a time-invariant intensity profile across its thickness (chopped CW lasers are better suited owing to their greater beam-pointing stability). Raffel et al. (1996) applied their technique to successfully measure the three-dimensional flow under a disk rotating in glycerine.

Another single camera technique was proposed by Herpfer and Jeng (1995) wherein the out-of-plane velocity was obtained by particle streaks. The in-plane velocity was obtained by double-pulsing a pulsed laser with coinciding sheets. A third laser sheet (centered with respect to, and somewhat thicker than the double-pulsed sheets) from a CW laser produces particle pathlines whose lengths are determined by the sheet thickness. Thus, each particle is recorded as a particle-pair superposed on its streak trajectory. The streak length divided by the in-plane velocity provided the residence time of the particle in the CW laser sheet; the out-of-plane velocity was obtained by dividing the CW sheet thickness with this residence time. Not all streak/pair combinations were usable, but the probability of valid combinations could be improved by tuning the system parameters. However, the data density is rather low as in most particle streak methods, and furthermore, the method cannot be applied to complicated flows without a large out-of-plane component.

Halloin and Jottrand (1994) provide a variation of the above method in which particles were illuminated by multiple bursts of light from a chopped Ar–Ion laser formed into a sheet such that each particle produces a streak consisting of a series of dashes. The laser bursts were coded to determine which of the three types of streaks were valid. The out-of-plane component is determined by counting the number of dashes in each valid streak. For acceptable accuracy, at least five dashes are required; the technique suffers from the usual particle tracking limitations, as well as low dynamic range. Some ambiguity results because the edges of the light sheet are not sharp.

Willert and Gharib (1992) placed a mask containing three pin holes in front of a single CCD camera equipped with a 25 mm diameter lens to accomplish three-dimensional measurements (these measurements were made over a thin volume rather than a plane). Pinholes of 1 mm diameter formed an equilateral triangle with 6 mm sides and produced triplet images for each particle. The technique required the use of deliberate defocusing of the image to determine the three-dimensional position of individual particles. For each triplet, a centroid was calcu-

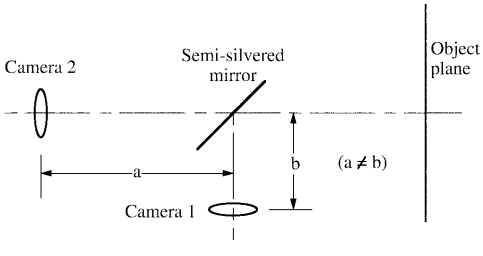

Fig. 9. An in-line stereoscopic arrangement (adapted from Grant et al. 1995)

lated as well as the average separation between the corner points. From this, they were able to deduce the three-dimensional trajectories of particles seeded into a vortex ring impinging against a wall. Willert and Gharib (1992) report an error in the out-of-plane measurement that was 40 times greater than the in-plane measurement. This large error arises from the small off-axis angle $\approx d/d_o$ of this method, where d is the pinhole separation. Furthermore, data density is low because individual triplets must be tracked. Although the forward-scatter arrangement used here greatly increases the light scattering efficiency of the particles, the mask blocks a sizable fraction of scattered light from reaching the sensor.

Stolz and Köhler (1994) also employed defocusing to extract the out-of-plane component. The light sheet was oriented orthogonally to the camera axis as usual, but was located beyond the focal plane such that particles always remained out of focus. Particles in the light sheet closer to the focal plane produced smaller images according to

$$\Delta z = f^{\#}\,\frac{1+M}{M^2}\,\Delta D$$

where ΔD is the change in the particle image diameter caused by an out-of-plane displacement Δz; M is the nominal magnification and $f^{\#}$ is the f-number. The technique requires up to five consecutive exposures during the particles' residence in the light sheet in order to drive the standard deviation in the out-of-plane velocity down to 10%. Again, the data density is rather low.

Cenedese and Paglialunga (1989) used parallel, partially overlapping light sheets of different colors to extract the out-of-plane velocity. Their beams had gaussian intensity profiles with $\sigma = 0.5$ mm and a peak-to-peak separation of 0.2 mm. A particle travelling in the out-of-plane direction would produce images with appropriately varying green and blue intensities. The ratio of these intensities yields the out-of-plane velocity.

In a similar manner, Dinkelacker et al. (1992) determined the out-of-plane component using particle tracking inside a 3 mm thick light sheet whose intensity varied in an exponential manner across its thickness. Thus, by measuring the intensity of a particle image at two instants in time, the out-of-plane displacement could be calculated.

3 Error analysis

Arroyo and Greated (1991), Prasad and Adrian (1993a), and Lawson and Wu (1997a) present error analyses for the translation system. Lawson and Wu (1997a), and Zang and Prasad (1997) present error analyses for the angular displacement system (the latter included the Scheimpflug condition in their angular displacement arrangement). Of these, the results of Lawson and Wu (1997a) include the variation of error with off-axis position.

Following standard methods of error analysis, the uncertainties in the calculated displacements (Eqs. 3–5) can be related to the uncertainties in the geometric parameters of the stereocamera. Assuming that each of the variables is uncorrelated and distributed with a standard deviation, σ, and perfect registration, we have:

$$\left[\frac{\sigma_{\Delta z}}{\Delta z}\right]^2 = (\sigma_{\Delta X_1}^2 + \sigma_{\Delta X_2}^2)\left[\frac{d_o}{M_n S \Delta z}\right]^2 + \left[\frac{\sigma_S}{S}\right]^2 + \left[\frac{\sigma_{M_n}}{M_n}\right]^2 + \left[\frac{\sigma_{d_o}}{d_o}\right]^2 \tag{6}$$

$$\left[\frac{\sigma_{\Delta x}}{\Delta x}\right]^2 = \left[\frac{\sigma_{\Delta X_1}(x-\frac{S}{2})}{M_n S \Delta x}\right]^2 + \left[\frac{\sigma_{\Delta X_2}(x+\frac{S}{2})}{M_n S \Delta x}\right]^2 + \left[\frac{\sigma_{M_n}}{M_n}\right]^2 + \left[\frac{\sigma_S}{S}\frac{\Delta z}{\Delta x}\frac{x}{d_o}\right]^2 + \left[\frac{\sigma_x}{d_o}\frac{\Delta z}{\Delta x}\right]^2 \tag{7}$$

$$\left[\frac{\sigma_{\Delta y}}{\Delta y}\right]^2 = (\sigma_{\Delta X_1}^2 + \sigma_{\Delta X_2}^2)\left[\frac{y}{M_n S \Delta y}\right]^2 + (\sigma_{\Delta Y_1}^2 + \sigma_{\Delta Y_2}^2) \times \left[\frac{1}{2M_n \Delta y}\right]^2 + \left[\frac{\sigma_{M_n}}{M_n}\left(1 + \frac{\Delta z y}{\Delta y d_o}\right)\right]^2 + \left[\frac{\sigma_S}{S}\frac{\Delta z}{\Delta y}\frac{y}{d_o}\right]^2 + \frac{1}{2}\left[\frac{\sigma_y}{d_o}\frac{\Delta z}{\Delta y}\right]^2 \tag{8}$$

Of the uncertainties listed above, $\sigma_{\Delta X_j}$ and $\sigma_{\Delta Y_j} (j = 1, 2)$ arise purely from the interrogation of the PIV photograph. They include *random* and *bias* errors as described by Prasad et al. (1992). The remaining uncertainties, viz., $\sigma_x, \sigma_y, \sigma_S, \sigma_{M_n}$, and σ_{d_o} are due to errors in measuring the various distances in the stereocamera. It is useful to study the dependence of the error in the calculated displacements resulting purely from PIV interrogation errors. Assuming $\sigma_{\Delta X_1} = \sigma_{\Delta X_2} = \sigma_{\Delta Y_1} = \sigma_{\Delta Y_2} = \sigma_{\Delta X}$, we have:

$$\sigma_{\Delta z} \approx \sqrt{2}\left[\frac{d_o}{MS}\right]\sigma_{\Delta X}$$

$$\sigma_{\Delta x} \approx \frac{1}{\sqrt{2}}\left[\frac{1}{M}\right]\sigma_{\Delta X} \qquad (\text{for } x = 0)$$

$$\sigma_{\Delta y} \approx \frac{1}{\sqrt{2}}\left[\frac{1}{M}\right]\sigma_{\Delta X} \qquad (\text{for } y = 0)$$

Thus, the relative error in the out-of-plane component (for $x = 0, y = 0$) reduces to:

$$\frac{\sigma_{\Delta z}}{\sigma_{\Delta x}} = \frac{\sigma_{\Delta z}}{\sigma_{\Delta y}} = 2\frac{d_o}{S} = \frac{1}{\tan\theta} \tag{9}$$

The relative error in the out-of-plane component is therefore obtained very simply as the reciprocal of the tangent of the off-axis half-angle θ (Fig. 3). While the above analysis pertains to the translation system, the analysis of Zang and Prasad (1997) showed that the Scheimpflug angular displacement system also exhibits the identical variation of out-of-plane error with θ. The absolute value of in-plane error is smaller (by $1/\sqrt{2}$) than the corresponding value for the single camera arrangement because two cameras contribute equally to the final result. Of course, the stereo arrangement also removes perspective error which can be quite sizable in single camera PIV.

Lawson and Wu (1997a) present the variation in the relative out-of-plane error as a function of the off-axis position x/d_o. As shown in Fig. 10a for the translation system, the relative error decreases rapidly with off-axis

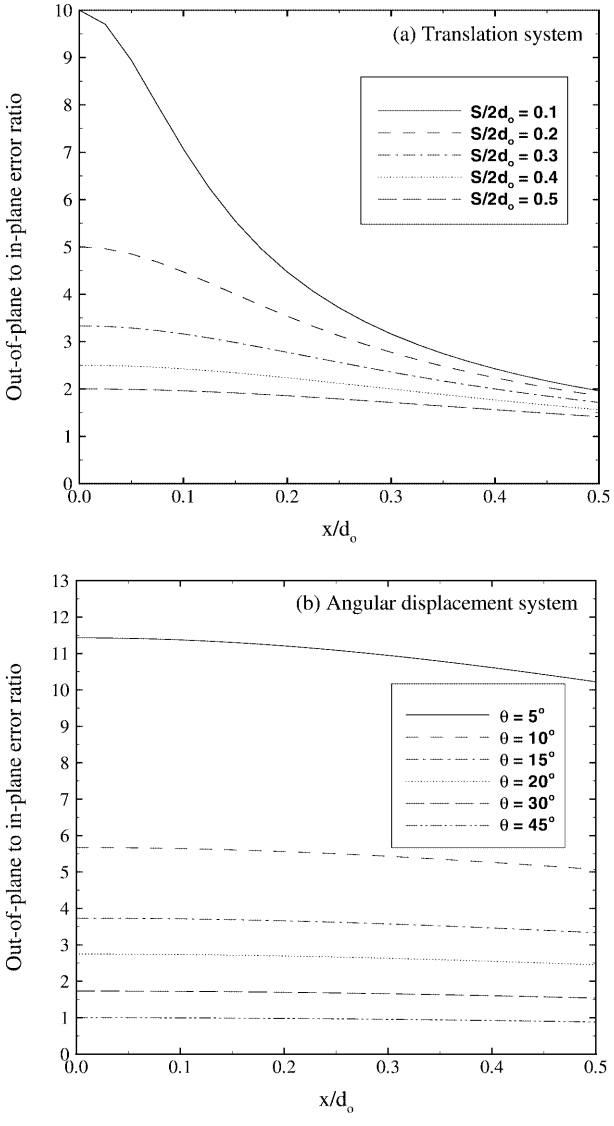

Fig. 10a, b. Variation of out-of-plane to in-plane error ratio with off-axis position (and $y = 0, z = 0$) for **a** translation system, and **b** angular displacement system; data is from Lawson and Wu (1997a)

position when $S/2d_o = \tan\theta < 0.2$, i.e., $\theta < 10°$, but becomes more-or-less invariant with larger off-axis angles. For the angular displacement system (Fig. 10b) the error is a weak function of off-axis position for the range analyzed ($5° \leq \theta \leq 45°$).

In order to balance the in-plane and out-of-plane errors, an off-axis half-angle of 45° is desirable; however, larger angles cause greater non-uniformity in magnification. Hill et al. (1999) used $\theta = 20°$, Willert (1997) used $\theta = 35°$, and Westerweel and van Oord (1999) employed $\theta = 45°$; Lawson and Wu (1997b) employed a range of θ values up to 45°.

It should be noted that, the above analysis completely ignores *registration error* which results when the two contributing views are improperly matched after back-projection on to the object plane. Such a mismatch, or misregistration, causes velocity information from different regions of the illuminated field to get combined leading to further errors. Misregistration will generally become more severe as the non-uniformity in magnification becomes large. Misregistration will depend on the sophistication of the algorithm used to back-project the image field into the object plane. While misregistration can be minimized with care, it is virtually impossible to completely eliminate it. In addition, registration errors are compounded if the flow contains significant spatial gradients.

Registration in expedited by placing markers in the flow field, or by exploiting features along physical boundaries in the field of view. Alternatively, Prasad and Adrian (1993a, b) proposed a Moiré method to register negatives from each camera. The current trend amongst stereo PIV practitioners is to use a calibration target in the flow field. In this case, registration is automatically accomplished (within the limits imposed by the accuracy of back-projection).

4
Reconstruction methods

Each view in a stereo-pair must be individually interrogated, typically, by means of a correlation analysis resulting in velocity data on a cartesian grid for each camera. The process of mapping the displacements from each image plane to the object plane and combining them to obtain the three-dimensional data is called reconstruction. The process of reconstruction can proceed along two different ways: (i) geometric reconstruction, and (ii) calibration-based reconstruction. Calibration-based reconstruction can be further classified as 2-d calibration-based reconstruction in which calibration precedes and simplifies geometric reconstruction, and 3-d calibration-based reconstruction in which a knowledge of system geometry is rendered unnecessary.

4.1
Geometric reconstruction

In order to project the displacements from the image plane, **X**, to the object plane, **x**, the following mapping is needed:

$$\mathbf{x} = \mathbf{f}(\mathbf{X}) \tag{10}$$

In the case of a translation system enjoying uniform magnification, the process of determining **f** is simplified. Unlike Fig. 6 which depicts a system with non-uniform magnification, the shaded areas for a symmetric translation system *will* coincide when mapped on to the object plane. Equations (3)–(5) can be used directly to combine the data after mapping. Input quantities are d_o, M_n, and S and the location and orientation of both sensors in three-dimensional space. Furthermore, one needs to project a given interrogation spot from the image plane on to the object plane accurately (the x and y-locations are required for determining Δx and Δy respectively). Such a reconstruction technique requires *a priori* knowledge of the complete recording geometry and is called geometric reconstruction (Fig. 11a). Geometric reconstruction was used for translation systems applied to air flow (Arroyo and Greated 1991) and translation tests in air (Prasad and Adrian 1993a).

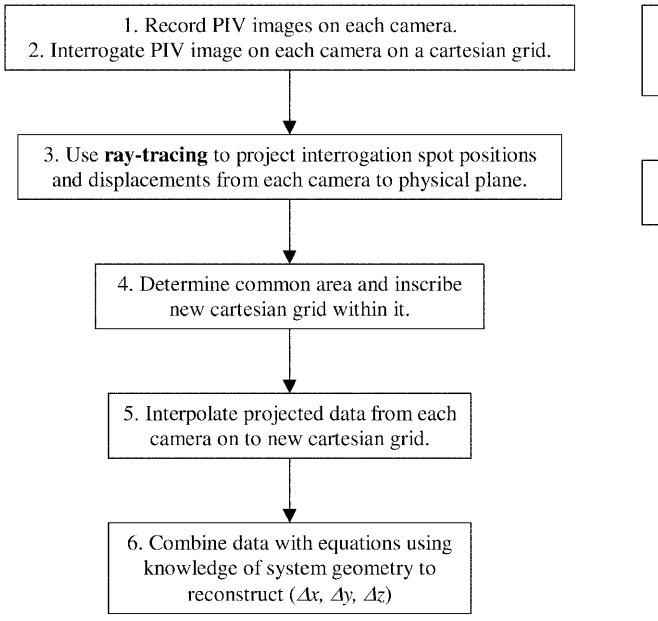

(a) geometric reconstruction

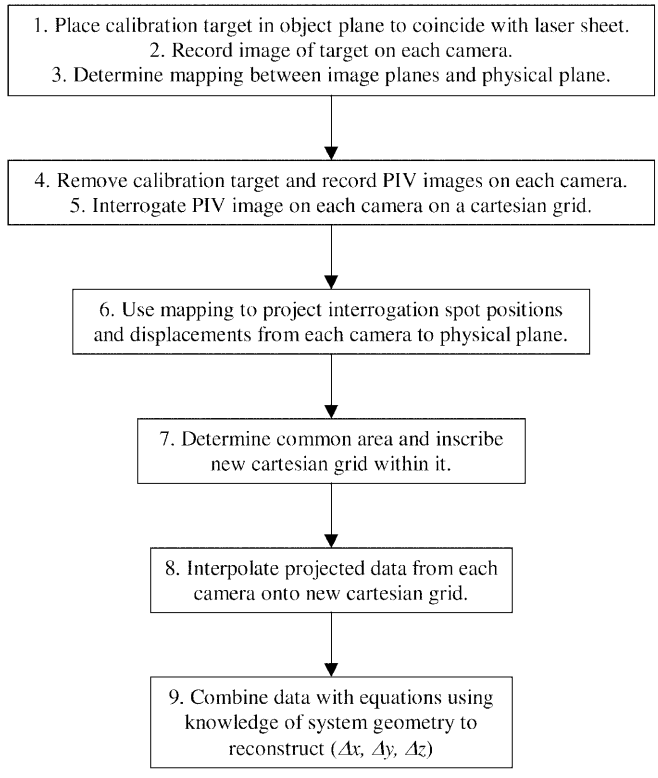

(b) 2-d calibration-based reconstruction

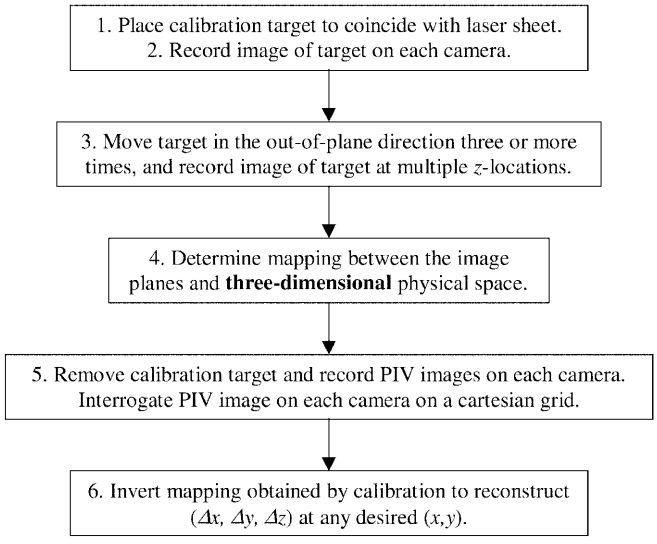

(c) 3-d calibration-based reconstruction

Fig. 11a–c. Steps involved in: **a** geometric reconstruction; **b** 2-d calibration-based reconstruction; and **c** 3-d calibration-based reconstruction

Geometric reconstruction becomes rapidly more complex when non-uniform magnifications are involved. Prasad and Adrian (1993a, b) accomplished geometric reconstruction for a translation system applied to a liquid flow, wherein images contained significantly varying magnification. They used a ray-tracing approach to map points on the titled image plane, through the lens and a thick liquid layer on to the object plane (the ray-tracing program accounted for the refraction of the ray at the liquid–air interface). The program required the depth of the liquid layer, M_n, d_o, the image plane tilt angle, and also the three-dimensional location of the film in each camera as inputs.

The ray-tracing program mapped the four corners of each cartesian interrogation grid into the object plane, resulting in partially overlapping, oppositely stretched trapezoids. First, the common area was determined and a new, cartesian grid was inscribed. Next, the displacement data from each cartesian grid in the image plane were interpolated on to the grid points of the newly inscribed grid in the object plane. Finally, the data from each camera were combined, however, Eqs. (3)–(5), could not be applied directly. Modified equations were developed to account for the refraction at the liquid–air interface (Prasad and Adrian 1993a). Similarly, Zang and Prasad (1997) used geometric reconstruction to evaluate the

performance of a Scheimpflug angular displacement system.

Geometric reconstruction is possible only when the geometry of the recording configuration is completely known and can be mathematically modeled, although it may be quite tedious. In some situations, such modeling may be impossible (for example, lens nonlinearity, or a misaligned CCD array). Furthermore, Eqs. (6)–(9) indicate that uncertainties from inaccurate system alignment such as $\sigma_x, \sigma_y, \sigma_S, \sigma_{M_n}$, and σ_{d_o} can increase the overall measurement error. Incorporation of the Scheimpflug condition and the presence of liquid–air interfaces can render geometric reconstruction even more demanding and error-prone. Therefore, it is worthwhile to consider an alternate method based on calibration which is more easily implemented and may produce more accurate results.

4.2 Calibration-based reconstruction

Calibration-based reconstruction may be further classified into 2-d or 3-d calibration methods. In the former, a mapping function is sought to relate each two-dimensional image plane to the two-dimensional object plane. In the latter, the mapping function provides a direct relationship between a particle location *in some 3-d neighborhood* of the object plane and its corresponding position on each image plane. While 2-d calibration methods still require a knowledge of the recording geometry to accomplish the final step of applying the reconstruction equations, 3-d calibration methods require no such input.

All calibration-based methods require the placement of a target in the object plane. The calibration-target is usually a plate containing a collection of dots arranged on a cartesian grid, or a cartesian grid with black line rulings. For example, Willert (1997) and Lawson and Wu (1997a) used rulings with 5 mm square spacing. Soloff et al. (1997) used a 12×12 cartesian grid of 1 mm diameter white circles with center-to-center spacing of 5 mm on a black background. Similarly, Westerweel and van Oord (1999) used a cartesian grid of black dots on a white background. The author has used a professional imagesetter (such as the Agfa Avantra 25) to print transparencies containing cartesian grids of white dots on a black background with resolutions of up to 3600 dpi. The target plate is placed inside the test-section to coincide exactly with the light sheet, and should be large enough to encompass the region of interest during flow measurements.

The stereocamera is aligned in its final configuration, and calibration commences by acquiring an image of the calibration target on each camera. The location of the grid points in the image plane is usually obtained by template-matching; the template must match the characteristic marks that represent the grid points on the original target. For example, in the case of the a target containing rulings, the intersection points are accurately located by cross-correlating with a + correlation mask (Willert 1997). The signal peak in the spatial cross-correlation plane is located to sub-pixel accuracy by means of a curve-fit. (The same steps are followed to obtain particle displacements during PIV interrogations.)

2-d calibration methods

As mentioned earlier, 2-d calibration provides a mapping between the two-dimensional object plane and each two-dimensional image plane. 2-d calibration essentially replaces the ray-tracing approach required in geometric reconstruction. The result of this procedure is a set of calibration data for each camera,

$$\mathbf{x}_i = \mathbf{f}(\mathbf{X}_i) \tag{11}$$

where $\mathbf{x}_i$ and $\mathbf{X}_i$ are corresponding points on the object and image planes respectively, and $i\ (= 1, 2, \ldots, n)$ is a counter for the number of grid-points on the original target. The next task is to determine the mapping function **f**. A first order mapping of the form

$$x = M_x X + C_x$$
$$y = M_y Y + C_y$$

cannot account for non-uniform magnifications, and other non-linearities (M, C above are the magnification and shift respectively).

Therefore, Westerweel and van Oord (1999) employed a second order mapping:

$$x = a_1 X^2 + a_2 Y^2 + a_3 XY + a_4 X + a_5 Y + a_6$$
$$y = b_1 X^2 + b_2 Y^2 + b_3 XY + b_4 X + b_5 Y + b_6$$

The coefficients $a_1, a_2, \ldots, a_6$ and $b_1, b_2, \ldots, b_6$ can be determined by solving the following equations using a least squares solution:

$$\mathbf{A}\begin{bmatrix} a_1 \\ a_2 \\ a_3 \\ a_4 \\ a_5 \\ a_6 \end{bmatrix} = \begin{bmatrix} x_1 \\ x_2 \\ \vdots \\ x_n \end{bmatrix}, \qquad \mathbf{B}\begin{bmatrix} b_1 \\ b_2 \\ b_3 \\ b_4 \\ b_5 \\ b_6 \end{bmatrix} = \begin{bmatrix} y_1 \\ y_2 \\ \vdots \\ y_n \end{bmatrix}$$

where

$$\mathbf{A} = \mathbf{B} = \begin{bmatrix} X_1^2 & Y_1^2 & X_1 Y_1 & X_1 & Y_1 & 1 \\ X_2^2 & Y_2^2 & X_2 Y_2 & X_2 & Y_2 & 1 \\ \vdots & \vdots & \vdots & \vdots & \vdots & \vdots \\ X_n^2 & Y_n^2 & X_n Y_n & X_n & Y_n & 1 \end{bmatrix}$$

As a result, any point in the image plane can be uniquely mapped to a point in the object plane, and the calibration process is complete. The procedure can be easily extended to higher-order as only a set of linear equations must be solved.

Next, the calibration target is removed and stereo images of the flow are recorded and interrogated on a cartesian grid in the image plane. Using the same mapping coefficients, the displacement data from each camera are also projected into the object plane. The data are then interpolated on to the final, cartesian grid in the object plane using a routine which interpolates data from a non-square grid to a square grid. The data are finally combined using the standard equations to obtain $\Delta x, \Delta y$, and Δz.

Willert (1997) employed two mapping methods and compared the results from each. The first technique listed below maps a rectangle into a trapezoid, i.e., the straightness of lines is preserved:

$$x = \frac{a_{11}X + a_{12}Y + a_{13}}{a_{31}X + a_{32}Y + a_{33}}$$
$$y = \frac{a_{21}X + a_{22}Y + a_{23}}{a_{31}X + a_{32}Y + a_{33}}$$

The second technique uses higher-order terms and can compensate for additional distortions:

$$x = \frac{a_{11}X + a_{12}Y + a_{13} + a_{14}X^2 + a_{15}Y^2 + a_{16}XY}{a_{31}X + a_{32}Y + a_{33} + a_{34}X^2 + a_{35}Y^2 + a_{36}XY}$$
$$y = \frac{a_{21}X + a_{22}Y + a_{23} + a_{24}X^2 + a_{25}Y^2 + a_{26}XY}{a_{31}X + a_{32}Y + a_{33} + a_{34}X^2 + a_{35}Y^2 + a_{36}XY}$$

In the above, $a_{33} = 1$. Willert (1997) reports that the determination of the mapping coefficients by means of a linear least-squares method is not straightforward. Instead, he used a nonlinear least-squares method to determine the 8 or 17 coefficients. Willert reports that the second, higher-order method did not produce noticeably better results in his case, which he attributes to the lack of geometric distortions in the imaging lenses. In a significant departure from other calibration-based reconstruction techniques, Willert (1997) used the image-to-object mapping in a different, unique way: Instead of interrogating the particle images first and mapping the displacements to the object field (as done by Westerweel and Nieuwstadt (1991), Westerweel and van Oord (1999), and others), he directly mapped the *image fields containing particle images to the object plane* and performed the interrogations there on the final cartesian grid. Subsequently, the displacements from each camera were combined to produce the required three-dimensional vectors.

2-d calibration-based reconstruction was used by Westerweel and Nieuwstadt (1991), Willert (1997), Lawson and Wu (1997b), Synnergren (1997), Westerweel and van Oord (1999), and Lecerf et al. (1999). 2-d calibration provides particles displacements as seen by each camera on the final cartesian grid in the object plane without requiring any knowledge of the recording geometry. However, as Fig. 11b shows, the final step of determining $(\Delta x, \Delta y, \Delta z)$ uses reconstruction equations (see for example, Eqs. 3–5) that *still require some knowledge of the geometry* such as separation between lenses, object distance, the angular orientation of the camera axis to the object plane (in the case of Willert 1997) and so on. Therefore, it may be concluded that in 2-d calibration-based reconstruction, calibration precedes and facilitates the final reconstruction step wherein back-projected data are combined using equations which still require the recording geometry as inputs. As mentioned earlier, such quantities pertaining to the recording geometry may be difficult to measure, and could introduce errors. Furthermore, if recording is accomplished through a liquid–air interface, the reconstruction equations will need to be modified to account for refraction at the interface (unless a liquid prism is used to restore paraxial recording, as in the case of Westerweel and van Oord 1999). 3-d calibration-based reconstruction, discussed next, provides an alternative approach.

3-d calibration methods

In contrast to 2-d calibration, the approach followed by Soloff et al. (1997) does not require knowledge of the system geometry at any stage during reconstruction (Fig. 11c). This is because their procedure acquired calibration data at not one, but three different z-locations: (i) the calibration target was located at the object plane, (ii) the target was placed slightly behind, but parallel to, the object plane, and (iii) the target was placed in front of the object plane. The z-separation between the calibration planes was comparable to the light sheet thickness.

Then, the relationship between the three-dimensional object field position $\mathbf{x}$ and its two-dimensional image field for each camera $\mathbf{X}$ could be written as:

$$\mathbf{X} = \mathbf{F}(\mathbf{x}) \tag{12}$$

where $\mathbf{F}$ was approximated by the following polynomial expression (Soloff et al. 1997):

$$\begin{aligned}\hat{\mathbf{F}}(x) = {} & \mathbf{a}_0 + \mathbf{a}_1 x_1 + \mathbf{a}_2 x_2 + \mathbf{a}_3 x_3 + \mathbf{a}_4 x_1^2 \\ & + \mathbf{a}_5 x_1 x_2 + \mathbf{a}_6 x_2^2 + \mathbf{a}_7 x_1 x_3 + \mathbf{a}_8 x_2 x_3 \\ & + \mathbf{a}_9 x_3^2 + \mathbf{a}_{10} x_1^3 + \mathbf{a}_{11} x_1^2 x_2 + \mathbf{a}_{12} x_1 x_2^2 \\ & + \mathbf{a}_{13} x_2^3 + \mathbf{a}_{14} x_1^2 x_3 + \mathbf{a}_{15} x_1 x_2 x_3 \\ & + \mathbf{a}_{16} x_2^2 x_3 + \mathbf{a}_{17} x_1 x_3^2 + \mathbf{a}_{18} x_2 x_3^2\end{aligned}$$

where $\mathbf{a}_i$ are vector-valued coefficients determined by a least squares approach: 4 sets of a_i are required, one each for $X_1^{(1)}$, $X_2^{(1)}$, $X_1^{(2)}$, and $X_2^{(2)}$, where the superscripts denote cameras 1 and 2. In the above expression, (x_1, x_2, x_3) are used to represent the physical coordinates in place of (x, y, z), and (X_1, X_2) for the image plane coordinates (X, Y). This polynomial has a cubic dependence in x_1 and x_2 and a quadratic dependence on x_3 (because only three z planes were used in the calibration; additional planes in z would permit higher order terms in x_3).

Following the analysis of Soloff et al. (1997), the particle image displacement given by

$$\mathbf{\Delta X} = \mathbf{F}(\mathbf{x} + \mathbf{\Delta x}) - \mathbf{F}(\mathbf{x})$$

may be approximated as

$$\mathbf{\Delta X} \approx \mathbf{\nabla F}(\mathbf{x})\mathbf{\Delta x}$$

where

$$(\mathbf{\nabla F})_{ij} = \frac{\partial F_i}{\partial x_j} = F_{i,j}$$

where $i = 1, 2$ and $j = 1, 2, 3$. Then,

$$\begin{bmatrix} \Delta X_1^{(1)} \\ \Delta X_2^{(1)} \\ \Delta X_1^{(2)} \\ \Delta X_2^{(2)} \end{bmatrix} = \begin{bmatrix} F_{1,1}^{(1)} & F_{1,2}^{(1)} & F_{1,3}^{(1)} \\ F_{2,1}^{(1)} & F_{2,2}^{(1)} & F_{2,3}^{(1)} \\ F_{1,1}^{(2)} & F_{1,2}^{(2)} & F_{1,3}^{(2)} \\ F_{2,1}^{(2)} & F_{2,2}^{(2)} & F_{2,3}^{(2)} \end{bmatrix} \begin{bmatrix} \Delta x_1 \\ \Delta x_2 \\ \Delta x_3 \end{bmatrix} \tag{13}$$

The required three-dimensional displacements are determined from this final expression. Equation (13) reiterates the observation in Sects. 1 and 2 that the stereoscopic arrangement provides four equations for three unknowns. In typical symmetric stereocameras, symmetry considerations reveal that the second and fourth equations in

Eq. (13) may be averaged to improve the accuracy of Δx_2 as indicated in Sect. 2. If such a reduction is not obvious in more general situations, Eq. (13) may be solved using a least-squares approach (Soloff et al. 1997).

In summary, the approach followed by Soloff et al. (1997) does not require the input of the recording geometry at any stage, and is therefore best suited for recording geometries which cannot be easily mathematically modeled.

Soloff et al.'s (1997) 3-d calibration approach was applied by Hill et al. (1999) to the flow around a Rushton turbine. However, Hill et al. used five z-planes for calibration instead of three planes used by Soloff et al. (1997) which allowed a quartic fit in z, whereas a cubic fit was retained for the in-plane coordinates. Similarly, Bjorkquist (1998) employed up to nine z-planes separated by 0.5 mm for 3-d calibration.

4.3
Current trends and recommendations

While large-format film remains an indispensable medium for situations demanding very high spatial resolution, the popular trend in PIV today is to use CCD sensors as the recording medium. For a stereoscopic system employing a Scheimpflug condition, a mechanism is needed to allow the user to tilt the camera lens-axis with respect to the CCD sensor axis. Willert (1997), and Westerweel and van Oord (1999) used a specially built "tilt-adapter" to set the correct angle. Commercial systems such as TSI (1998) and Dantec (1998) also include such a tilt-adapter to satisfy the Scheimpflug condition; both systems use calibration-based reconstruction, which according to recent literature, is the preferred a reconstruction method.

On a cautionary note, Willert (1997) reports that for all calibration-based methods, it is crucial to ensure that the target plate during calibration coincides exactly with the laser sheet during flow recording. Willert's unique approach of mapping the particle image fields directly to the object plane enabled him to test the accuracy of alignment in a straightforward manner. The procedure consisted of recording two views of the flow at the *same* time instant using a single laser pulse, mapping each particle image field to the object plane, and cross-correlating the mapped images from camera 1 with that of camera 2. An ideal alignment should produce a field with every vector having zero magnitude. However, his measured vector field showed deviations in excess of 10 pixels towards the edges, although the reconstructed grids overlapped better than 1 pixel. In his configuration, a rotation of less than 0.6° was sufficient to produce a measured horizontal misalignment of ten pixels, leading to a misregistration between the two camera views of up to 1 mm. Willert (1997) recommends the use of a more reliable calibration scheme which can ensure a better alignment of the calibration target with the light sheet.

The current literature does not reveal any other investigations of errors due to such misalignments. There exists a need for a thorough error-analysis of 2-d and 3-d calibration-based reconstruction systems.

In general, calibration-based reconstruction allows for greater ease and flexibility while setting up the stereoscopic PIV experiment. Consider a purely geometric method in which one needs to measure the recording geometry completely, including $S,\ d_o,\ \theta$, and also the location and orientation of both sensors in three-dimensional space. In contrast, for 2-d calibration-based methods, the sensors' locations and orientations are rendered unnecessary by the process of calibration, which greatly simplifies the implementation. Consequently, 2-d calibration methods are immune to certain image plane imperfections and misalignments which could adversely affect geometric reconstruction. Because the remaining geometric quantities are required as inputs in the reconstruction equations, 2-d calibration-based stereocameras must still be fabricated with requisite care. For 3-d calibration-based methods, an explicit knowledge of system geometry is completely unnecessary as this information is automatically incorporated into the object-space $\Rightarrow$ image-plane mapping function. For the latter purely calibration-based methods, one need not, for example, ensure even a high degree of symmetry between the two cameras. Such imperfections are rendered harmless by the process of 3-d calibration.

5
Summary

The principle of stereoscopic PIV has been presented. The technique of using two cameras has been compared and contrasted with non-stereoscopic methods to obtain three-dimensional vectors on planar domains. Amongst the two broad classes of stereoscopic arrangements, the Scheimpflug angular displacement method offers higher accuracy, but at the cost of non-uniform magnification. The error in the out-of-plane component relative to the in-plane component is equal to $1/\tan\theta$ where θ is the included half-angle. Two reconstruction methods have been reviewed – geometric, and calibration-based (2-d as well as 3-d). Geometric reconstruction requires a complete knowledge of the recording geometry. In contrast, 2-d calibration-based reconstruction requires only a partial knowledge of the recording geometry, whereas 3-d calibration-based reconstruction requires no such knowledge. Calibration-based reconstruction is simpler to implement and may be less susceptible to errors than geometric reconstruction, especially if the recording geometry is complex (involving liquid-air inter-faces or non- uniform magnifications). In some cases where the recording geometry cannot be mathematically modeled, calibration is unavoidable. The current trend in stereoscopic PIV seems to favour the use of CCD cameras arranged in the Scheimpflug angular displacement configuration and the use of calibration-based reconstruction.

References

Adrian RJ (1991) Particle-imaging techniques for experimental fluid mechanics. Ann Rev of Fluid Mech 23: 261–304

Altenhofen RE (1952) Rectification. In: Manual of Photogrammetry. American Society of Photogrammetry, Washington, DO, p 457

Arroyo MP; Greated CA (1991) Stereoscopic particle image velocimetry. Meas Sci Technol 2: 1181–1186

Bjorkquist D (1998) Design and calibration of a stereoscopic particle image velocimetry system. Proc 9th Int Symp on Appl of Laser Techniques to Fluid Mech, pp 6.5.1–6.5.8
Cenedese A; Paglialunga A (1989) A new technique for the determination of the third velocity component with PIV. Exp Fluids 8: 228–230
Dantec (1998) Dantec announces the world's first commercial 3D PIV system. Dantec Newsletter 5(3): 2–3
Dinkelacker F; Schäfer M; Ketterle W; Wolfrum J; Stolz W; Köhler J (1992) Determination of the third velocity component with PTA using an intensity graded light sheet. Exp Fluids 13: 357–359
Gauthier V; Riethmuller ML (1988) Application of PIDV to complex flows: measurements of the third component. In: VKI-LS 1988–06 Particle image displacement velocimetry. Von Karman Institute for Fluid Mechanics, Rhode-Saint-Genese, Belgium
Gaydon M; Raffel M; Willert C; Rosengarten M; Kompenhans J (1997) Hybrid stereoscopic particle image velocimetry. Exp Fluids 23: 331–334
Grant I; Zhao Y; Tan Y; Stewart JN (1991) Three component flow mapping: experiences in stereoscopic PIV and holographic velocimetry. In: Dybbs A; Ghorashi B (eds) Laser anemometry advances and applications, vol. 1, ASME, New York, pp 365–371
Grant I; Fu S; Pan X; Wang X (1995) The application of an in-line, stereoscopic, PIV system to 3-component velocity. Exp Fluids 19: 214–221
Halloin VL; Jottrand R (1994) A new technique for the experimental study of 3D velocity fields. Exp Fluids 17: 115–118
Herpfer DC; Jeng SM (1995) Planar measurement of three-component velocity by streaked-particle-imaging velocimetry. App Opt 34: 2301–2304
Hill DF; Sharp KV; Adrian RJ (1999) Stereoscopic particle image velocimetry measurements of the flow around a Rushton turbine. Submitted to Exp Fluids
Hinsch KD (1995) Three-dimensional particle velocimetry. Meas Sci Technol 6: 742–753
Jacquot P; Rastogi PK (1981) Influence of out-of-plane deformation and its elimination in white light speckle photography. Opt Lasers Eng 2: 33–55
Lawson NJ; Wu J (1997a) Three-dimensional particle image velocimetry: error analysis of stereoscopic techniques. Meas Sci Technol 8: 894–900
Lawson NJ; Wu J (1997b) Three-dimensional particle image velocimetry: experimental error analysis of a digital angular stereoscopic system. Meas Sci Technol 8: 1455–1464
Lecerf A; Renou B; Allano D; Boukhalfa A; Trinité M (1999) Stereoscopic PIV: validation and application to an isotropic turbulent flow. Exp Fluids 26: 107–115
Liu Z-C; Adrian RJ; Meinhart CD; Lai W (1997) Structure of a turbulent boundary layer using stereoscopic, large-format video-PIV. In: Adrian RJ; Durao DFG; Durst F; Heitor MV; Maeda M; Whitelaw JH (eds) Developments in laser techniques and fluid mechanics. Springer, Berlin Heidelberg, pp 259–273
Prasad AK; Adrian RJ; Landreth CC; Offutt PW (1992) Effect of resolution on the speed and accuracy of particle image velocimetry interrogation. Exp Fluids 13: 105–116
Prasad AK; Adrian RJ (1993a) Stereoscopic particle image velocimetry applied to liquid flows. Exp Fluids 15: 49–60
Prasad AK; Adrian RJ (1993b) Investigation of non-penetrative thermal convection using stereoscopic particle image velocimetry. In: Cha SS; Trolinger JD (eds) Optical diagnostics in fluid and thermal flow (Proc. SPIE 2005), pp 667–682
Prasad AK; Jensen K (1995) Scheimpflug stereocamera for particle image velocimetry in liquid flows. Appl Opt 34: 7092–7099
Raffel M; Westerweel J; Willert C; Gharib M; Kompenhans J (1996) Analytical and experimental investigations of dual-plane particle image velocimetry. Opt Eng 35: 2067–2074
Sinha SK (1988) Improving the accuracy and resolution of particle image or laser speckle velocimetry. Exp Fluids 6: 67–68
Sinha SK; Kuhlman PS (1992) Investigating the use of stereoscopic particle streak velocimetry for estimating the three-dimensional vorticity field. Exp Fluids 12: 377–384
Soloff SM; Adrian RJ; Liu Z-C (1997) Distortion compensation for generalized stereoscopic particle image velocimetry. Meas Sci Technol 8: 1441–1454
Stolz W; Köhler J (1994) In-plane determination of 3D-velocity vectors using particle tracking anemometry (PTA). Exp Fluids 17: 105–109
Synnergren P (1997) Measurement of three-dimensional displacement fields and shape using electronic speckle photography. Opt Eng 36: 2302–2310
TSI (1998) On-line, Stereoscopic PIV system. Flow Profiles 7(1): 2
Westerweel J; Nieuwstadt FTM (1991) Performance tests on 3-dimensional velocity measurements with a two-camera digital particle-image velocimeter. In: Dybbs A; Ghorashi B (eds) Laser anemometry advances and applications, vol 1, ASME, New York, pp 349–355
Westerweel J; van Oord J (1999) Stereoscopic PIV measurements in a turbulent boundary layer. In: Stainslaus M; Kompenhans J; Westerweel J (eds) Particle image velocimetry: progress toward industrial application. Kluwer, Dordrecht
Willert C (1997) Stereoscopic digital particle image velocimetry for application in wind tunnel flows. Meas Sci Technol 8: 1465–1479
Willert CE; Gharib M (1992) Three-dimensional particle imaging with a single camera. Exp Fluids 12: 353–358
Zang W; Prasad AK (1997) Performance evaluation of a Scheimpflug stereocamera for stereoscopic particle image velocimetry. App Opt 36: 8738–8744